B: Biomaterials, Surfactants, and Membranes

Rheology of Membrane-Attached Minimal Actin Cortices

Helen Noeding, Markus Schoen, Corinna Kramer, Nils Doerrer, Aileen Kuerschner, Burkhard Geil, Ingo P. Mey, Claus Heussinger, Andreas Janshoff, and Claudia Steinem

J. Phys. Chem. B, **Just Accepted Manuscript** • DOI: 10.1021/acs.jpcb.7b11491 • Publication Date (Web): 28 Mar 2018

Rheology of Membrane-Attached Minimal Actin Cortices

Helen Nöding [†#], Markus Schön[‡#], Corinna Reinermann[‡], Nils Dörrer [†], Aileen Kürschner[‡], Burkhard Geil [†], Ingo Mey[‡], Claus Heussinger[§], Andreas Janshoff [†*] and Claudia Steinem[‡*]

[†]Georg August Universität Göttingen, Institut für Physikalische Chemie, Tammannstr. 6, 37077 Göttingen, Germany

[‡]Georg August Universität Göttingen, Institut für Organische und Biomolekulare Chemie, Tammannstr. 2, 37077 Göttingen, Germany

[§]Georg August Universität Göttingen, Institut für Theoretische Physik, Friedrich-Hund-Platz 1, 37077 Göttingen, Germany

[#]both authors contributed equally to this work

ABSTRACT: The actin cortex is a thin cross-linked network attached to the plasma membrane, being responsible for the cell's shape during migration, division and growth. In a reductionist approach, we created a minimal actin cortex (MAC) attached to a lipid membrane to correlate the filamentous actin architecture with its viscoelastic properties. The system is composed of a supported 1-palmitoyl-2-oleoyl-*sn*-glycero-3-phosphocholine (POPC) bilayer doped with the receptor lipid phosphatidylinositol(4,5)-bisphosphate (PtdIns(4,5)P_2) to which a constitutively active mutant of ezrin, being a direct membrane-cytoskeleton linker, is bound. The formation of the MAC on the supported lipid bilayer is analyzed as a function of increasing PtdIns(4,5)P_2/ezrin pinning points revealing an increase in the intersections between actin filaments, i.e., the node density of the MAC. Bead tracking microrheology on the membrane attached actin network provides information about its viscoelastic properties. The results show that ezrin serves as a dynamic cross-linker for the actin cortex attached to the lipid bilayer and that the stiffness of the network is influenced by the pinning point density, relating the plateau storage modulus G_0 to the node density of the MAC.

KEYWORDS: cytoskeleton mechanics, ezrin, lipid bilayer, passive microrheology, phosphoinositide

INTRODUCTION

The actomyosin cytoskeleton is at the heart of many cell and tissue shape changes, but linking molecular-scale organization to viscoelastic properties remains a challenge. Several models have been developed to explain the different phenomena uncovered in the rheological behaviors of cells. The actomyosin within the cell has been treated as a single-phase material,[1,2] as a poroelastic material[3] or soft glassy rheology models have been applied.[4,5] Among the various models, poroelasticity stands out to actually explicitly consider the contribution from the cytoplasm to the rheological properties of living cells. A particularly important part of the eukaryotic actin cytoskeleton that largely contributes to the mechanical properties of living cells is the actin cortex[6] being connected to the plasma membrane via dynamic protein linkers and thereby being responsible for cell motility and remodeling as well as signal transduction processes and endocytosis.[7] The ezrin-radixin-moesin (ERM) proteins are the major architects of this cell cortex, as they directly link the plasma membrane to the underlying cortical actin cytoskeleton.[8] ERM proteins are found in the cytosol in an inactive, so called "dormant" conformation. To connect the plasma membrane with the actin cortex, ERM proteins need to be activated, which is achieved by binding to the lipid phosphatidylinositol(4,5)-bisphosphate (PtdIns(4,5)P_2) via the N-terminal ERM association domain (N-ERMAD) and a phosphorylation of a threonine located at the C-terminal ERM association domain (C-ERMAD).[8–10] For ezrin, phosphorylation of threonine 567 is known to induce a transition from inactive ezrin oligomers to active membrane-associated monomers that act as cross-linkers between the plasma membrane and the actin cortex.[11] This membrane anchorage impacts the structural and material properties of the cell cortex[12] along with actin cross-linkers, actin-capping and severing proteins, molecular motors as well as matrix and cell-cell-adhesion proteins. Several studies have, however, brought up the discussion that a mere modulation of the actin architecture, such as thickness, connectivity and filament orientation, can already considerably affect the cell surface tension,[6,13–15] while a recent work of Eggeling and coworkers[16] suggests that changes in actin patterning alter membrane architecture but occur functionally independent of macroscopic cortex elasticity.

To be able to pin down the contribution of the individual components of the complex actin cortex attached to the plasma membrane and relate its architecture to the mechanical properties, a minimal system with membrane-bound actin filaments mimicking an actin cell cortex is highly desirable. In recent years such minimal actin cortices (MACs) providing a planar geometry based on supported lipid bilayers have been developed, however, most established systems are based on artificial linkages between the membrane and the actin network. Murrell and coworkers localized F(filamentous)-actin and myosin II to the surface of a supported lipid bilayer by the crowding agent methylcellulose or they combined the crowding agent with a His_{10}-tagged fimbrin bound to a Ni^{2+}-chelating lipid DGS-NTA embedded in a supported lipid bilayer.[13,17] Schwille and coworkers as well as Honigmann *et al*. reported on MACs based on actin/actomyosin networks linked via neutravidin/streptavidin-biotin to a lipid bilayer.[18,19] Köster and coworkers used a semi-physiological linker, i.e., a His_{10}-tagged engineered membrane actin linker based on native ezrin to form a model cortex.[20] While these

studies all focused on the actomyosin dynamics, mechanical studies, particularly frequency dependent viscoelastic measurements, on MACs are still missing.

In general, the viscoelastic properties of F-actin and actin binding proteins are investigated in 3D F-actin solutions.[21–23] However, these model systems do not capture the native spatial organization of the actin cortex attached to a membrane. Here, we report on a MAC, in which the F-actin network is bound via ezrin/PtdIns(4,5)P_2 linkages to the lipid bilayer. By a combination of fluorescence microscopy and video particle tracking based microrheology, we correlate the architecture of the networks with their viscoelastic properties and discuss the impact of linker dynamics on the rheological properties.

METHODS

Preparation of minimal actin cortices. Silicon substrates (1.0 × 2.0 cm² with 100 nm silicon dioxide, Silicon Materials, Kaufering, Germany) were hydrophilized in a $H_2O/NH_3/H_2O_2$ (5:1:1, *v*/*v*) solution for 20 min at 70 °C. The substrate was then placed in a Teflon chamber, buffer solution was added (50 mM KCl, 20 mM Na-citrate, 0.1 mM EDTA, 0.1 mM NaN_3, pH 4.8)[24] and immediately incubated with small unilamellar vesicles (SUVs) (0.8 mg/mL) for one hour. SUVs composed of POPC, PtdIns(4,5)P_2 (Avanti Polar Lipids, Alabaster, AL, United States) doped either with Atto390-1,2-dioleoyl-*sn*-glycero-3-phosphoethanolamine (Atto390-DOPE, ATTO-TEC, Siegen, Germany) or TexasRed-1,2-diphytanoyl-*sn*-glycero-3-phosphoethanolamine (DHPE) (TexasRed-DHPE, Sigma-Aldrich) were obtained by sonification (cycle 4, 60%, 30 min) for one hour. After spreading of the lipid bilayer, the surface was rinsed with buffer solution followed by a buffer exchange (50 mM KCl, 20 mM Tris, 0.1 mM EDTA, 0.1 mM NaN_3, pH 7.4). The protein ezrin T567D, recombinantly expressed in *Escherichia coli* cells (strain BL21(DE3)pLysS) as described previously,[25] was bound at a final concentration of 1 µM at 4 °C overnight. Non-bound protein was removed by rinsing with buffer solution changing to a buffer suited for F-actin binding (50 mM KCl, 20 mM Tris, 2 mM $MgCl_2$, 0.1 mM NaN_3, pH 7.4). For pre-polymerized F-actin networks, non-muscle G-actin (c_a = 10 mg/mL, Cytoskeleton, Denver, CO, USA) was dissolved in G-buffer (5 mM Tris/HCl, 0.2 mM $CaCl_2$, 0.1 mM NaN_3, pH 7.4) to reach a final concentration of 0.4 mg/mL. After addition of dithiothreitol (0.5 mM) and ATP (0.2 mM) the solution was stored on ice for one hour avoiding oligomers. Subsequent centrifugation (17,000×*g*, 20 min, 4 °C) was used to remove possible oligomers. After adding carboxylate-modified polystyrene latex beads with a diameter of d = 2 µm (1 µL containing 0.8 % solids, Sigma-Aldrich), which bind nonspecifically to the polymer network,[26] and vortexing, polymerization was induced by adding 10 % of the total volume of polymerization solution (500 mM KCl, 20 mM $MgCl_2$, 20 mM ATP, pH 7.0). After 30 min of polymerization time, 0.01 mol% (referred to G-actin monomers) of AlexaFluor488-phalloidin (λ_{ex} = 488 nm) was added to label the actin filaments. The resulting F-actin solutions obtained under the experimental polymerization conditions were analyzed by atomic force microscopy (details are described in the Supporting Information). These filamentous actin networks containing polystyrene beads were then incubated for 4.5 hours on protein-decorated lipid bilayers.

Subsequent rinsing with buffer (50 mM KCl, 20 mM Tris, 2 mM $MgCl_2$, 0.1 mM NaN_3, pH 7.4) removed unbound filaments.

Fluorescence imaging and network analysis. Confocal fluorescence images were taken with an upright confocal laser scanning microscope (Olympus, FV 1200; Olympus, Hamburg, Germany) equipped with a 405 nm diode laser (50 mW), a 488 nm diode laser (50 mW) and a diode pumped solid state laser emitting at 561 nm (20 mW) and a water immersion objective (60 x, LPUMPlanN, NA = 1.0, Olympus). The membrane associated fluorophore Atto390-DOPE was excited at λ_{ex} = 405 nm and detected at 425-475 nm, while TexasRed-DHPE was excited at λ_{ex} = 561 nm and detected at 580-640 nm. The AlexaFluor488-phalloidin labelled F-actin was excited at λ_{ex} = 488 nm and detected at 500-545 nm. For excitation of the tracker particles an excitation wavelength of λ_{ex} = 561 nm was used and the fluorescence emission was detected at 575-675 nm. For image analysis of the actin networks, an 'artificial retina' was applied to generate skeletal networks (for details see Supporting Information).

Fluorescence recovery after photobleaching (FRAP). The fluorescence intensity of a region of interest of a lipid bilayer doped with TexasRed-DHPE was bleached by a short laser pulse (λ_{bleach} = 561 nm) and the time dependent fluorescence recovery was recorded with a frame rate of 3 frames per second. Almost full recovery was observed in all experiments confirming the presence of a fluid lipid bilayer with only a small immobile fraction. FRAP experiments were either performed on lipid bilayers lacking an attached actin network or with an attached minimal actin cortex. The resulting diffusion coefficients were calculated using a Hankel transformation.[27]

Microrheology. Fluorescent carboxylate-modified polystyrene latex beads with a diameter of d = 2 µm were used for video particle tracking. The integration of the beads into the networks was confirmed by fluorescence microscopy (Supporting Information). Videos of 100,000 images were recorded with a sCMOS camera (Zyla-5.5-CL-10, Andor Oxford Instruments, Belfast, UK) mounted on a fluorescence microscope (Olympus, FV 1200; Olympus, Hamburg, Germany) equipped with a 60× objective (LPUMPlan N, NA = 1.0, Olympus, Hamburg, Germany) with 50 frames per second. About 1-10 beads could be recorded in each video with a high spatiotemporal resolution allowing to track movements in the subpixel regime. Tracking, calculation of the time averaged mean squared displacements (MSDs) and determination of the complex shear moduli was accomplished by a tracking algorithm by John Crocker and theory by Weitz and coworkers.[28,29] MSDs were ensemble averaged. A model described by Plagge *et al*. was used to model the microrheological data.[30]

RESULTS AND DISCUSSION

Organization of F-actin on a fluid membrane is a function of pinning point density. A minimal actin cortex (MAC) was formed by attaching a pre-polymerized F-actin network to an ezrin decorated supported lipid bilayer composed of 1-palmitoyl-2-oleoyl-*sn*-glycero-3-phosphocholine (POPC) and the receptor lipid for ezrin, PtdIns(4,5)P_2 (Figure 1A). An ezrin

mutant (ezrin T567D)[11] instead of the wild type was used to mimic the phosphorylated state of the protein ensuring that the membrane bound proteins are in a constitutively active state.[31,32]

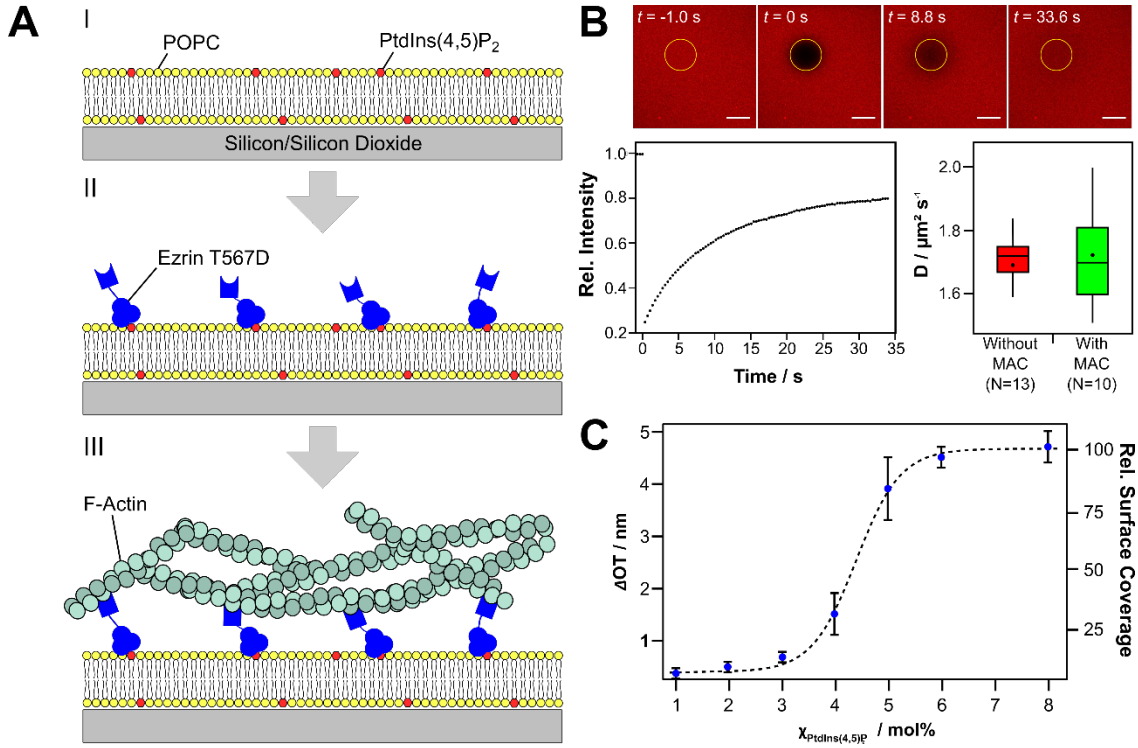

Figure 1. (**A**) Schematic illustration of the preparation of a minimal actin cortex (MAC). Small unilamellar vesicles composed of POPC and PtdIns(4,5)P_2 are spread on a silicon/silicon dioxide substrate to achieve a continuous planar lipid bilayer (**I**). The active mutant of ezrin (ezrin T567D) is specifically bound to PtdIns(4,5)P_2 (**II**), followed by the attachment of a pre-polymerized F-actin network (**III**). (**B**) Fluorescence recovery after photobleaching (FRAP) experiments document the fluidity of the membrane in the absence and presence of membrane attached actin filaments. (Top) Fluorescence images of a supported bilayer doped with 0.4 mol% TexasRed-DHPE before (t = -1 s), right after the bleach (t = 0 s), and during the recovery process (t = 8.8 s and 33.6 s) The region of interest is marked by a yellow circle from which the time-dependent fluorescence intensity is read out (bottom left). Scale bar: 10 µm. (Bottom right) Diffusion coefficients for lipid bilayers without MAC were determined to be D = (1.7 ± 0.1) µm²·s^{-1}. Lipid bilayers with an attached MAC exhibited identical diffusion coefficients of D = (1.7 ± 0.2) µm²·s^{-1}. (**C**) Change in optical thickness (ΔOT) upon binding of ezrin T567D to a POPC bilayer as a function of the PtdIns(4,5)P_2 content $\chi_{PtdIns(4,5)P2}$. A maximum ΔOT = 4.3 nm was measured for a PtdIns(4,5)P_2 content larger than 6 mol%, which corresponds to a physical thickness of 3.0 nm taking the refractive index of a protein layer into account.[33] The maximum ΔOT was used to set the protein surface coverage to 100 %.

Spreading of small unilamellar vesicles on a silicon/silicon dioxide surface results in continuous fluid lipid bilayers composed of POPC and PtdIns(4,5)P_2 as revealed by fluorescence micrographs and fluorescence recovery after photobleaching experiments (Figure 1B). The obtained diffusion coefficients of 1.7 µm²·s^{-1} are consistent with a fluid lipid bilayer,[24,27] which is not altered by attaching an F-actin network to the membrane. Reflectometric interference spectroscopy (RIfS)[34,35] was used to monitor the adsorption of ezrin T567D on these supported bilayers as a function of different of PtdIns(4,5)P_2 concentrations in a non-invasive and label-free fashion. We chose a PtdIns(4,5)P_2 concentration range which is compatible with that reported in the plasma membrane.[36] The total membrane composition of a cell generally consists of about 1 mol% PtdIns(4,5)P_2, while it can achieve high local concentrations of 5 mol%. Our results show that with increasing PtdIns(4,5)P_2 in the membrane, the ezrin surface

coverage increases sigmoidally up to 6 mol% PtdIns(4,5)P_2 (Figure 1B), where it remains constant indicating full coverage of the membrane with ezrin, the expected jamming limit, which was set to 100% coverage.

F-actin networks bind specifically to the ezrin-decorated membranes as visualized by confocal laser scanning fluorescence microscopy (Figure 2B/C). Defects in the membrane (Figure 2A/C, black area in the top right) remain free of F-actin indicating that there is no non-specific interaction between the network and the silicon support. *Z*-stack images (Figure 2D) of the membrane-attached network show that it is very thin, independent of the number of PtdIns(4,5)P_2 pinning sites in the membrane with a thickness below the axial resolution of about 1 µm.[37] From the *z*-stack images we infer a mean extension of the fluorescence intensity of 1.5 ± 0.3 µm (*N* = 11) suggesting that the MAC is thinner than 1 µm as expected for non-cross-linked networks attached to a ezrin-decorated membrane surface. The thickness is thus in the same order of magnitude than the average cortex thickness of 200 nm of living cells.[6]

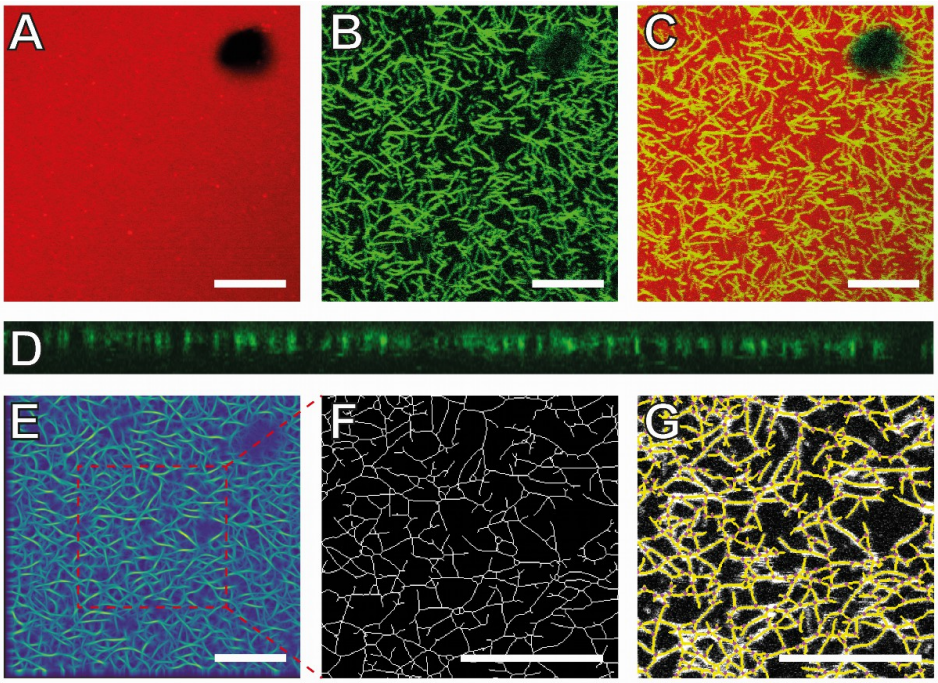

Figure 2. Images showing the organization of a membrane attached F-actin network. (**A**) A continuous lipid bilayer composed of POPC/PtdIns(4,5)P_2 (96.6:3) and doped with 0.4 mol% TexasRed-DHPE (red) was formed on a silicon surface. (**B**) After binding of ezrin T567D, a pre-polymerized F-actin network labeled with AlexaFluor488-phalloidin (green) was attached to it. (**C**) Overlay of the membrane (red) and the F-actin network (green). (**D**) Cross section (image stacks in *z*-direction) of the membrane attached F-actin network (total height 1 µm). (**E**) 'Artificial retina' analysis and (**F**) skeletonization of the F-actin network based on (**E**). (**G**) Result of the node analysis. The yellow lines show the skeletonized actin network reproduced from (**F**) with the identified nodes depicted in red, which is overlaid with the original fluorescence image (white color). Scale bars: 5 µm (bottom right).

With the MAC in hand, we were then able to address the question how the number of pinning sites, i.e., the amount of bound ezrin attached to PtdIns(4,5)P_2 influences the architecture of the F-actin network. To get access to quantitative parameters of the network as a function of pinning sites, each fluorescence image was subjected to an 'artificial retina' analysis (Figure 2E, further details can be found in the Supporting Information) greatly facilitating

skeletonization of the filaments (Figure 2F). The critical point of the 'artificial retina' analysis is the optical enhancement of filamentous structures prior to thresholding and skeletonization. This enhancement is achieved by applying a stack of convolutional filters to the raw image (Figure 2B) where the motive of the individual filters is sensitive for rod-like local structures of various orientations and thicknesses in the raw image intensities (Figure 2). The pixel-wise maximum filter response values obtained by such a convolution quantify the filamentous character (i.e., thickness, length, orientation and curvature) of the local environment and with a suitable color encoding they produce a clean, smooth, and highly de-noised image of the filament structure (Figure 2E). We call this technique 'artificial retina' owing to its extremely strong bias towards filamentous intensity structures and blindness for any other motive. Images obtained by the 'artificial retina' are well suited for standard skeletonization algorithms followed by typical network morphology analysis methods. The resulting skeleton provides parameters of the network such as intersections between filaments, termed nodes (Figure 2G) as well as the mesh size of the network obtained by a subsequent bubble analysis (see Supporting Information). We found that mesh size estimation through bubble analysis was more prone to errors particularly for sparse networks and overestimates smaller meshes. Therefore, we mainly refer to the node density, which is a reliable parameter to describe the network density.

Figure 3 shows the impact of PtdIns(4,5)P_2 content on the network architecture. With increasing PtdIns(4,5)P_2 concentration, which results in an increased ezrin surface coverage (Figure 1C), the network becomes denser mirrored in the determined node density. The node density of the actin network increases with the PtdIns(4,5)P_2 concentration, i.e., the pinning point density *P* in the membrane (Figure 3B).

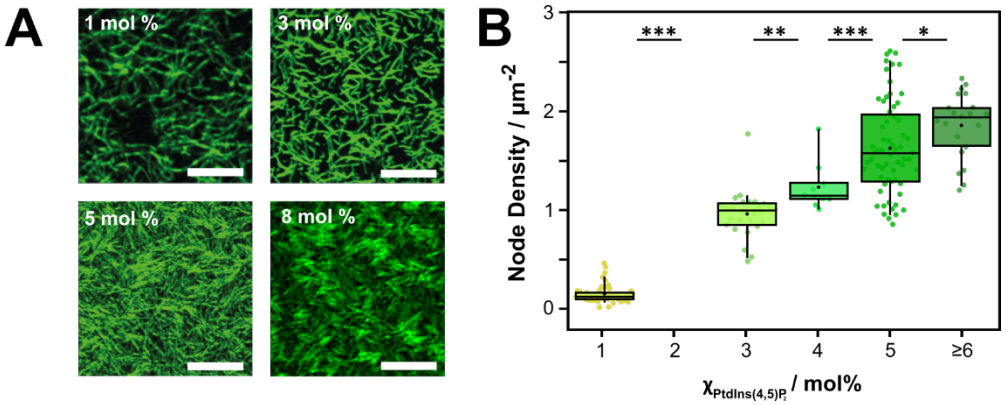

Figure 3. F-actin network architecture as a function of PtdIns(4,5)P_2 concentration in the membrane. (**A**) Exemplary fluorescence micrographs of MACs (F-actin labeled with AlexaFluor488-phalloidin shown in green) attached to membranes differing in the PtdIns(4,5)P_2 concentration. Scale bar: 5 µm (bottom right). **(B)** Node density of membrane attached F-actin networks as a function of the PtdIns(4,5)P_2 concentration $\chi_{PtdIns(4,5)P2}$ in the lipid bilayer. Box plots extend from the 25th to the 75th percentile, whiskers from the 5th to the 95th. For the analysis *n* images from *m* preparations were used. 1 mol%: *n*= 63, *m* = 3; 3 mol%: *n* = 27, *m* = 6; 4 mol%: *n* = 10, *m* = 2; 5 mol%: *n* = 64, *m* = 7; ≥ 6 mol%: *n* = 30, *m* = 4. A two-sample Welch's *t*-test was performed to test the null hypothesis that the data of the indicated datasets are from populations with equal means. (*) indicates that the null hypothesis, the means of two populations are equal, was rejected at the 5% significance level, (**) at the 1% significance level and (***) at the 0.1% significance level. The two-tailed *P*-values are: <10^{-4} for 1 mol% and 3 mol%, 0.0072 for 3 mol% and 4 mol%, 0.0005 for 4 mol% and 5 mol%, and 0.016 for 5 mol% and >6 mol%. The same significance levels hold also for the Mann-Whitney *U* test.

Node densities obtained on membranes with $\chi_{PtdIns(4,5)P2} \geq 6$ mol% are basically identical within the error of the experiment, consistent with the notion that the ezrin coverage is saturated at $\chi_{PtdIns(4,5)P2} = 6$ mol% (Figure 1C). F-actin networks attached to membranes harboring ≥6 mol% PtdIns(4,5)P_2 show a twentyfold increase in node density (1.96 ± 0.45 nodes/μm^2) compared to 1 mol% PtdIns(4,5)P_2. The node density ν scales almost linearly with the pinning point density $\chi_{PtdIns(4,5)P2}$ in the membrane ($\nu \propto \chi_{PtdIns(4,5)P2}^{1.1}$). As mentioned above, we found that the node density estimation was more reliable than analyzing the mesh sizes of the F-actin networks especially for sparse networks that are obtained at 3 mol% PtdIns(4,5)P_2 and lower (see Supporting Information).[38] Membranes with 3 mol% PtdIns(4,5)P_2 show an average mesh size of 0.8 ± 0.5 μm, which is about 4 times larger than natural cortices from living cells, where actin networks are strongly cross-linked and nucleators like formin and Arp2/3 are present.[39,40] Furthermore, we analyzed the order parameter[41] of the networks demonstrating that the actin networks attached to a lipid bilayer are isotropically oriented for all PtdIns(4,5)P_2 densities (see Supporting Information).

Frequency dependent viscoelastic properties of MACs. To relate the F-actin architecture to the viscoelastic properties of the membrane attached networks, we performed video particle tracking based microrheology using a bead size of r = 1 μm small enough to be compliant with the actin mesh size but also large enough to realize a decent signal-to-noise ratio for precise tracking. This method enabled us to assess the complex shear modulus $G^*(f) = G'(f) + iG''(f)$ of the MAC in a broad frequency regime.[28] Figure 4 shows the storage modulus G' and the loss modulus G'' as a function of frequency for an entangled 3D actin network (Figure 4A) and the MAC with two different pinning point densities (Figure 4B/C). The spectra of the 3D F-actin network show distinct frequency regimes: (1) a plateau region, where the elastic response dominates over the viscous contribution ($G' > G''$), (2) a high frequency regime typically showing a power law scaling with an exponent of 0.75, which is dominated by single filament mechanics and, (3) a low frequency regime, where dynamic processes related to diffusion and opening and closing of non-covalent bonds prevail.

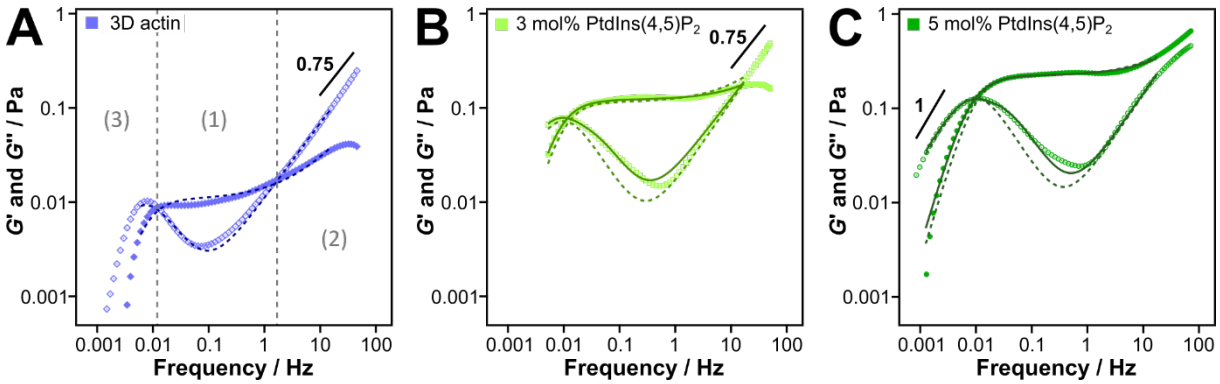

Figure 4. Frequency dependent viscoelastic properties of MACs. The frequency dependent storage modulus G' (filled symbols) and loss modulus G'' (open symbols) are shown together with the fit according to the theoretical model adopted from Plagge *et al.*[30] (see text for details). The dashed lines correspond to one type of cross-links giving rise to a single relaxation time (one Maxwell element, eqs. (7) and (8)), while the solid lines represent the fit according to two types of cross-links with distinct relaxation times (two Maxwell elements, eqs. (10) and (11),

solid lines) (for all parameters see Supporting Information, Table S2). (**A**) Entangled (3D) F-actin networks (8-23 μM G-actin), N = 5. (**B**) F-actin network attached via ezrin T567D to a lipid membrane containing (**B**) 3 mol% PtdIns(4,5)P_2, N = 6 and (**C**) 5 mol% PtdIns(4,5)P_2, N = 9. N is the number of averaged bead trajectories. The power law scaling behavior with an exponent of 0.75 is shown in (**A**) and (**B**) as a solid black line; in (**C**) the low frequency dependency with a slope of 1 is shown as solid line. For the model comprising only one type of cross-link (dashed lines) the relaxation time is given by $\tau = \eta/G_0$ for (**A**): $\tau = 139 \pm 15$ s, (**B**): $\tau = 103 \pm 12$ s and (**C**): $\tau = 103 \pm 6$ s. Two cross-links (solid lines) lead to relaxation times for (**B**): $\tau_1 = 121 \pm 9$ s, $\tau_2 = 28 \pm 4$ s and for (**C**): $\tau_1 = 131 \pm 16$ s, $\tau_2 = 33 \pm 6$ s.

These three regimes were not only found in 3D networks but were also recapitulated in the quasi two-dimensional F-actin networks attached to a membrane (Figure 4B/C). From regime (1), the magnitude of the storage modulus in the plateau region, the plateau modulus G_0, was extracted, which reports on the stiffness of the system. For entangled 3D F-actin networks, we found a plateau modulus of G_0(3D actin) = 9 mPa (median), which is about three times lower than previously reported plateau moduli for similar concentrations.[42] The absolute values, however strongly depend on the preparation of the networks and on the setup calibration. Attachment of these F-actin networks to a lipid membrane results in significant stiffening of the composite material compared to the purely entangled 3D F-actin networks (Figure 5). A 14-fold increase of the plateau modulus upon binding of actin networks to a PtdIns(4,5)P_2 containing lipid membrane mediated by ezrin (G_0(3 mol% PtdIns(4,5)P_2) = 0.133 Pa (median)) was observed. A mere increase in F-actin density at the surface can hardly explain this significant increase in G_0. We suggest that the confinement of the movement of the actin filaments via the 'cross-linker' ezrin to the lipid membrane mainly governs the increased G_0 value, i.e., the overall stiffness of the MAC. The effectiveness of a cross-linker in its ability to strengthen the resulting networks is usually expressed in a power law scaling of the plateau modulus $G_0 \propto R^x$, with the relative cross-linker concentration $R = c_{cross}/c_a$ (c_{cross} = cross-linker concentration, c_a = G-actin concentration). For cross-linkers in 3D networks $x \approx 2$.[43] We assume that the pinning point density $\chi_{PtdIns(4,5)P2}$ in the membrane given by the amount of PtdIns(4,5)P_2 is equivalent to R. For the two PtdIns(4,5)P_2 concentrations we find a relation of $G_0 \propto (\chi_{PtdIns(4,5)P2})^{1.5}$. The power law coefficient x is lower than that found for 3D networks but larger than what has been reported for F-actin networks attached to lipid monolayers by a biotin-streptavidin linkage.[44] For these systems a linear relationship with $G_0 \propto \chi^{1.0}$ was reported. Simulation studies further revealed a power law scaling of the plateau modulus on the cross-linking density of $G_0 \propto \chi^{1.0}$ in 2D networks for affinely deforming networks.[45] We have shown that the density of node points ν scales approximately linear with the pinning point density in the membrane (Figure 3A). Together with the dependency of the plateau modulus on the pinning point concentration we find a scaling behavior of the plateau modulus with the number of nodes of G_0(PtdIns(4,5)P_2) $\propto \nu^{1.5}$. This scaling is similar to that predicted for non-affine 3D F-actin networks (G_0(3D actin) $\propto c_a^{7/5}$).[46]

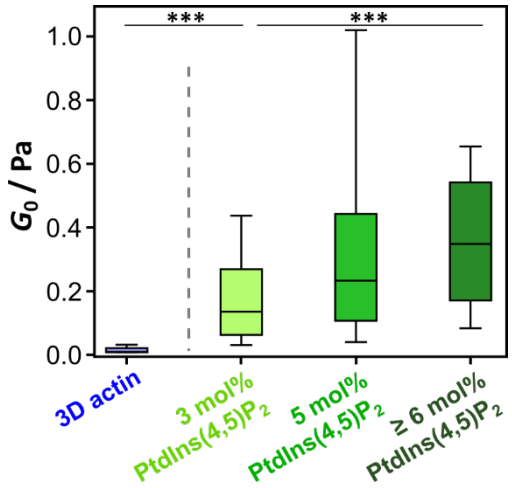

Figure 5. Plateau modulus G_0 as a function of pinning point density. 3D actin: Entangled F-actin network (8-23 μM, median: 0.009 Pa), N = 8. 3 mol % PtdIns(4,5)P_2: F-actin attached via ezrin T567D to a lipid membrane containing 3 mol% PtdIns(4,5)P_2 (median: 0.135 Pa), N = 306. 5 mol % PtdIns(4,5)P_2: F-actin attached via ezrin T567D to a lipid membrane containing 5 mol% PtdIns(4,5)P_2 (median: 0.233 Pa), N = 14. ≥6 mol % PtdIns(4,5)P_2: F-actin attached via ezrin T567D to a lipid membrane containing ≥6 mol% PtdIns(4,5)P_2 (median: 0.348 Pa), N = 243. Box plots extend from the 25th to the 75th percentile, whiskers from the 10th to the 90th. A Welch's *t*-test and a Mann-Whitney *U* test were performed to test the null hypothesis that the data of the indicated datasets are from populations with equal means. (***) indicates that the null hypothesis was rejected at the 0.1% significance level. The two-tailed *P*-values were <10^{-5} in either test.

In the high frequency regime (regime (1) in Figure 4), bending mode relaxations along the filament contribute to the viscoelastic response usually with a power law exponent of approximately 0.75.[47,48] In our experiments, we find power law scaling factors of the shear modulus of 0.60-0.84 in both the 3D actin samples as well as in the MACs. The power law scaling of the real part is altered for higher frequencies probably due to inertia effects.[49]

In the low frequency regime (regime (3) in Figure 4), relaxation of the elastically stored energy is observed in both the 3D actin sample and the membrane bound actin networks. This reduction of structural resistance to external forces can possibly originate from dynamic processes such as cross-linker unbinding or filament movement along its restricting tube.[21,48] The latter, called filament reptation, is dependent on the filament length. We thus shortened the mean filament length using gelsolin and indeed observed a shift in the cross-over frequency (Supporting Information) supporting the hypothesis that filament reptation causes the relaxation in the 3D networks. The average length in pure actin samples was estimated from the microrheological data and was found to be about 16μm (see Supporting Information).

We analyzed the spectral properties of our viscoelastic actin networks within the framework of a theory recently developed to describe reversibly cross-linked networks of semi-flexible polymers in a non-affine approach[30]. In brief, the actin filaments are assumed to be inextensible and the theory builds solely on linear bending deformations of a test filament in an effective medium formed by the surrounding network. This is justified since bending modes are by far softer than stretching of the filament. Therefore, the surrounding network essentially forms a 'tube-like' effective medium around the filament under consideration. The effective medium is represented by a harmonic potential acting on the test filament. A key

assumption is that straining of the network results in local positional changes of the tube rather than changes of the filament's contour length. It is further assumed that the effective medium couples to the filament under consideration only through its reversible cross-links, where thermal energy is comparable to the strength of a cross-link. Here, the cross-links are entanglement points and in the case of membrane attachment also the ezrin-mediated linkage to the membrane. As the lifetime of an ezrin-mediated bonding is in the range of seconds, we expect to see binding-unbinding kinetics in the rheological spectra as distinct relaxation times. The cross-links are assumed to exist in a rough periodic one-dimensional energy landscape distorted by external force rendering escape from the potential-well preferential in one direction through force-dependent rates. This implies that the rough energy landscape generates friction that can be represented by dashpot. As a consequence, the response function, which is the viscoelasticity of the effective medium, i.e., the actin network, consists of Maxwell elements. The number of elements depends on the number of types of cross-links with different binding-unbinding kinetics. In our case we expect to observe two types of cross-links, one simply formed by entanglement points and the other occurring due to binding of the actin network to the membrane via ezrin.

In essence, for one type of cross-link one can derive a simplified equation for the effective modulus G^*

$$\frac{1}{G^*} = \frac{1}{G_s} + \frac{1}{i\eta\omega}, \tag{1}$$

where η is the friction coefficient relating to cross-link binding/ unbinding, essentially identical to sliding along filaments. G_s is the modulus with permanent cross-links. It can be written as a sum over filament bending modes with wavenumber q_n (e.g. $q_n = n\pi/L$) as

$$\frac{1}{G_s} = \frac{1}{G_0}\sum_n \frac{\sin^2(q_n L/2)}{(Lq_n)^4 + i\omega/\omega_0}. \tag{2}$$

L is the contour length of the filament, G_0 the plateau modulus, and ω_0 the cross-over frequency to the high frequency branch. At high frequencies this gives the typical $G_s \sim (i\omega)^{3/4}$ scaling describing single filament mechanics and at low frequency a plateau at G_0. A simplified formula connecting the two limiting cases for the real part

$$G_s' \to G_0 \begin{cases} 0.38 \cdot \alpha_0 \cdot (\omega/\omega_0)^{3/4} & \omega \gg \omega_0 \\ 1 & \omega \ll \omega_0 \end{cases} \tag{3}$$

and the imaginary part

$$G_s'' \to G_0 \begin{cases} 0.92 \cdot \alpha_0 \cdot (\omega/\omega_0)^{3/4} & \omega \gg \omega_0 \\ (\omega/\omega_0) & \omega \ll \omega_0 \end{cases} \tag{4}$$

is given by:

$$G_s' = G_0\left(1 + 0.38 \cdot \alpha_0 \cdot (\omega/\omega_0)^{3/4}\right) \tag{5}$$

$$G_s'' = G_0 \cdot \left((0.92 \cdot \alpha_0)^{-1} \cdot (\omega/\omega_0)^{-3/4} + (\omega/\omega_0)^{-1}\right)^{-1} \tag{6}$$

Introducing a scaling parameter α_0 that originates in the summing over all modes. The numerical factors come from $i^{3/4}$. Splitting for real and imaginary part one writes

$$G' = (\eta\omega)^2 \cdot \frac{G_s'}{D} \quad (7)$$

$$G'' = \alpha_1 \eta\omega \cdot \frac{\left((G_s')^2 + G_s''(G_s'' + \eta\omega)\right)}{D} \quad (8)$$

with

$$D = (G_s')^2 + (G_s'' + \eta\omega)^2 \quad (9)$$

The parameter α_1 has been introduced to allow for shifting the imaginary part relative to the real part. This gives five fit parameters: G_0, ω_0, η, α_0 and α_1. The resulting fits to the experimental data are shown in Figure 4 as dashed lines. The time scale of unbinding is given by $\tau = \eta/G_0$. The theory generically reproduces the viscoelastic response of weakly deformed networks of the full frequency range capturing single filament dynamics as found for high frequency as well as diffusive motion and binding/unbinding kinetics at intermediate frequency. In particular for the membrane attached F-actin networks (Figure 4 B&C dashed line) it is clear that the right wing of the peak is broader than expected from merely a single Maxwell element. Thus, one expects additional time-scales that can be attributed to a specific linkage of the F-actin network to the surface to the membrane. Adding a second Maxwell element gives

$$G' = G_1' + \alpha_3 \cdot G_2' \quad (10)$$

and

$$G'' = G_1'' + \alpha_2 \cdot G_2''. \quad (11)$$

Two different scale factors α_3 and α_2 for real and imaginary parts were introduced since the real part does not show a clear second plateau due to the presence of a second Maxwell element. Thus, we find $\alpha_3 \ll \alpha_2$. The fit parameters now are G_0, ω_0, η_1, η_2 and the three scale parameters are α_0, α_1 and α_3. The full set of fitting parameters are given in the Supporting Information. The resulting fit is shown as solid line in Figure 4B&C.

The key finding here is that binding/unbinding kinetics of the membrane - actin linkers are displayed in the rheological data. The generic model suggests two Maxwell elements that we attribute to entanglement points and ezrin-mediated linkage of the network to the membrane. The off-rate corresponding to this ezrin-mediated linkage of the actin network to the lipid bilayer is around 0.03 s^{-1}, which is lower than recently reported for single molecule studies and *in vivo* work carried out by Fritsche *et al.*, but still realistic for moderately weak biological linkers.[12,32] Notably, the rebinding effect in our case might be quite substantially due to the strongly crowded situation, therefore effectively strengthening the bonding.

CONCLUSIONS

We found that the rheological properties of minimal actin cortices are largely governed by the dynamic attachment of actin to the lipid bilayer. We have demonstrated by fluorescence imaging and video particle tracking that both the architecture and the viscoelasticity of MACs can be adjusted by the number of pinning sites at the membrane. Pinning sites are realized by the amount of PtdIns(4,5)P_2 added to the lipid bilayer. PtdIns(4,5)P_2 serves as a natural

receptor for the cross-linker ezrin. The jamming limit of ezrin was found to be around 6 mol% of PtdIns(4,5)P_2. The network stiffens considerably with increasing number of pinning sites but also displays more intricate rheological properties than in 3D, which we could attribute to the reversible unbinding of the network to the membrane. Rheological data could well be fitted with a generic model exhibiting two relaxation times, one time constant representing entanglement points and the other one the ezrin-mediated cross-links.

ASSOCIATED CONTENT

Supporting Information. The Supporting Information is available free of charge on the ACS Publications website, Figures S1-S6, Table S1-S2 (pdf).

Data availability. The data that support the findings of this study is available upon request from the corresponding author.

AUTHOR INFORMATION

Corresponding authors

E-mail: ajansho@gwdg.de

E-mail: csteine@gwdg.de

Notes

The authors declare no competing financial interest.

Author contributions

M. S., A. K. and H. N. did the experiments and analyzed the data. I. M. helped with the MATLAB-assisted data analysis. B. G. and N. D. worked on the retina analysis. C. K. developed the model system. M. S., H.N., A. J. and C. S. wrote the manuscript. A. J. and C. S. designed the research. C. H. designed the model to fit the frequency dependent moduli.

ACKNOWLEDGEMENTS

This work was supported by the Deutsche Forschungsgemeinschaft (SFB 937, project A17 and A16). H. N. thankfully received a fellowship from the Deutsche Telekom Stiftung. We thank J. Gerber-Nolte for technical assistance, and K. Silbersdorff for preliminary work. We are thankful to M. Kilfoil for providing the microrheology software.

REFERENCES

1. Bausch, A. R.; Möller, W.; Sackmann, E. Measurement of Local Viscoelasticity and Forces in Living Cells by Magnetic Tweezers. *Biophys. J.* **1999**, *76,* 573–579.
2. Bursac, P.; Lenormand, G.; Fabry, B.; Oliver, M.; Weitz, D. A.; Viasnoff, V.; Butler, J. P.; Fredberg, J. J. Cytoskeletal Remodelling and Slow Dynamics in the Living Cell. *Nat. Mater.* **2005**, *4,* 557–561.
3. Moeendarbary, E.; Valon, L.; Fritzsche, M.; Harris, A. R.; Moulding, D. A.; Thrasher, A. J.; Stride, E.; Mahadevan, L.; Charras, G. T. The Cytoplasm of Living Cells Behaves as a Poroelastic Material. *Nat. Mater.* **2013**, *12,* 253–261.
4. Fabry, B.; Maksym, G. N.; Butler, J. P.; Glogauer, M.; Navajas, D.; Fredberg, J. J. Scaling the Microrheology of Living Cells. *Phys. Rev. Lett.* **2001**, *87,* 148102.

5. Deng, L.; Trepat, X.; Butler, J. P.; Millet, E.; Morgan, K. G.; Weitz, D. A.; Fredberg, J. J. Fast and Slow Dynamics of the Cytoskeleton. *Nat. Mater.* **2006**, *5,* 636–640.
6. Chugh, P.; Clark, A. G.; Smith, M. B.; Cassani, D. A. D.; Dierkes, K.; Ragab, A.; Roux, P. P.; Charras, G.; Salbreux, G.; Paluch, E. K. Actin Cortex Architecture Regulates Cell Surface Tension. *Nat. Cell Biol.* **2017**, *19,* 689–697.
7. Pollard, T. D.; Cooper, J. A. Actin, a Central Player in Cell Shape and Movement. *Science* **2009**, *326,* 1208–1212.
8. Zhu, L.; Zhou, R.; Mettler, S.; Wu, T.; Abbas, A.; Delaney, J.; Forte, J. G. High Turnover of Ezrin T567 Phosphorylation: Conformation, Activity, and Cellular Function. *Am. J. Physiol.* **2007**, *293,* C874-84.
9. Yonemura, S.; Matsui, T.; Tsukita, S.; Tsukita, S. Rho-Dependent and -Independent Activation Mechanisms of Ezrin/Radixin/Moesin Proteins: an Essential Role for Polyphosphoinositides In Vivo. *J. Cell Sci.* **2002**, *115,* 2569–2580.
10. Pearson, M. A.; Reczek, D.; Bretscher, A.; Karplus, P. Structure of the ERM Protein Moesin Reveals the FERM Domain Fold Masked by an Extended Actin Binding Tail Domain. *Cell* **2000**, *101,* 259–270.
11. Gautreau, A.; Louvard, D.; Arpin, M. Morphogenic Effects of Ezrin Require a Phosphorylation-Induced Transition from Oligomers to Monomers at the Plasma Membrane. *J. Cell Biol.* **2000**, *150,* 193–204.
12. Fritzsche, M.; Thorogate, R.; Charras, G. Quantitative Analysis of Ezrin Turnover Dynamics in the Actin Cortex. *Biophys. J.* **2014**, *106,* 343–353.
13. Murrell, M. P.; Gardel, M. L. F-Actin Buckling Coordinates Contractility and Severing in a Biomimetic Actomyosin Cortex. *P. Natl. Acad. Sci. USA* **2012**, *109,* 20820–20825.
14. Alvarado, J.; Sheinman, M.; Sharma, A.; MacKintosh, F. C.; Koenderink, G. H. Molecular Motors Robustly Drive Active Gels to a Critically Connected State. *Nat. Phys.* **2013**, *9,* 591–597.
15. Reymann, A.-C.; Boujemaa-Paterski, R.; Martiel, J.-L.; Guérin, C.; Cao, W.; Chin, H. F.; De La Cruz, Enrique M.; Théry, M.; Blanchoin, L. Actin Network Architecture Can Determine Myosin Motor Activity. *Science* **2012**, *336,* 1310–1314.
16. Fritzsche, M.; Li, D.; Colin-York, H.; Chang, V. T.; Moeendarbary, E.; Felce, J. H.; Sezgin, E.; Charras, G.; Betzig, E.; Eggeling, C. Self-Organizing Actin Patterns Shape Membrane Architecture but not Cell Mechanics. *Nat. Commun.* **2017**, *8,* 14347.
17. Murrell, M.; Gardel, M. L. Actomyosin Sliding is Attenuated in Contractile Biomimetic Cortices. *Mol. Biol. Cell* **2014**, *25,* 1845–1853.
18. Honigmann, A.; Sadeghi, S.; Keller, J.; Hell, S. W.; Eggeling, C.; Vink, R. A Lipid Bound Actin Meshwork Organizes Liquid Phase Separation in Model Membranes. *eLife* **2014**,, 1–16.
19. Heinemann, F.; Vogel, S. K.; Schwille, P. Lateral Membrane Diffusion Modulated by a Minimal Actin Cortex. *Biophys. J.* **2013**, *104,* 1465–1475.

20. Köster, D. V.; Husain, K.; Iljazi, E.; Bhat, A.; Bieling, P.; Mullins, R. D.; Rao, M.; Mayor, S. Actomyosin Dynamics Drive Local Membrane Component Organization in an In Vitro Active Composite Layer. *P. Natl. Acad. Sci. USA* **2016**, *113,* E1645-54.
21. Lieleg, O.; Claessens, M. M. A. E.; Luan, Y.; Bausch, A. R. Transient Binding and Dissipation in Cross-Linked Actin Networks. *Phys. Rev. Lett.* **2008**, *101,* 108101.
22. Gardel, M. L.; Shin, J. H.; MacKintosh, F. C.; Mahadevan, L.; Matsudaira, P.; Weitz, D. A. Elastic Behavior of Cross-Linked and Bundled Actin Networks. *Science* **2004**,, 1301–1305.
23. Koenderink, G. H.; Dogic, Z.; Nakamura, F.; Bendix, P. M.; MacKintosh, F. C.; Hartwig, J. H.; Stossel, T. P.; Weitz, D. A. An Active Biopolymer Network Controlled by Molecular Motors. *P. Natl. Acad. Sci. USA* **2009**, *106,* 15192–15197.
24. Braunger, J. A.; Kramer, C.; Morick, D.; Steinem, C. Solid Supported Membranes Doped with PIP2. Influence of Ionic Strength and pH on Bilayer Formation and Membrane Organization. *Langmuir* **2013**, *29,* 14204–14213.
25. Herrig, A.; Janke, M.; Austermann, J.; Gerke, V.; Janshoff, A.; Steinem, C. Cooperative Adsorption of Ezrin on PIP2-Containing Membranes. *Biochemistry-US* **2006**, *45,* 13025–13034.
26. Valentine, M. T.; Perlman, Z. E.; Gardel, M. L.; Shin, J. H.; Matsudaira, P.; Mitchison, T. J.; Weitz, D. A. Colloid Surface Chemistry Critically Affects Multiple Particle Tracking Measurements of Biomaterials. *Biophys. J.* **2004**, *86,* 4004–4014.
27. Jönsson, P.; Jonsson, M. P.; Tegenfeldt, J. O.; Höök, F. A Method Improving the Accuracy of Fluorescence Recovery after Photobleaching Analysis. *Biophys. J.* **2008**, *95,* 5334–5348.
28. Dasgupta, B. R.; Tee, S.-Y.; Crocker, J. C.; Frisken, B. J.; Weitz, D. A. Microrheology of Polyethylene Oxide Using Diffusing Wave Spectroscopy and Single Scattering. *Phys. Rev. E* **2002**, *65,* 51505.
29. Maria Kilfoil 'particle_pretracking_and_tracking_and_2D_feature_finding' & 'microrheology'. (accessed September, 2014). Available at http://people.umass.edu/kilfoil/downloads.html.
30. Plagge, J.; Fischer, A.; Heussinger, C. Viscoelasticity of Reversibly Crosslinked Networks of Semiflexible Polymers. *Phys. Rev. E* **2016**, *93,* 62502.
31. Shabardina, V.; Kramer, C.; Gerdes, B.; Braunger, J.; Cordes, A.; Schäfer, J.; Mey, I.; Grill, D.; Gerke, V.; Steinem, C. Mode of Ezrin-Membrane Interaction as a Function of PIP2 Binding and Pseudophosphorylation. *Biophys. J.* **2016**, *110,* 2710–2719.
32. Braunger, J. A.; Brückner, B. R.; Nehls, S.; Pietuch, A.; Gerke, V.; Mey, I.; Janshoff, A.; Steinem, C. Phosphatidylinositol 4,5-Bisphosphate Alters the Number of Attachment Sites Between Ezrin and Actin Filaments. A Colloidal Probe Study. *J. Biol. Chem.* **2014**, *289,* 9833–9843.
33. Vörös, J. The Density and Refractive Index of Adsorbing Protein Layers. *Biophys. J.* **2004**, *87,* 553–561.

34. Hänel, C.; Gauglitz, G. Comparison of Reflectometric Interference Spectroscopy with other Instruments for Label-Free optical detection. *Anal. Bioanal. Chem.* **2002**, *372,* 91–100.
35. Stephan, M.; Kramer, C.; Steinem, C.; Janshoff, A. Binding Assay for Low Molecular Weight Analytes Based on Reflectometry of Absorbing Molecules in Porous Substrates. *Analyst* **2014**, *139,* 1987–1992.
36. Martin, T. F. J. Role of PI(4,5)P(2) in Vesicle Exocytosis and Membrane Fusion. *Subcell. Biochem.* **2012**, *59,* 111–130.
37. Cole, R. W.; Jinadasa, T.; Brown, C. M. Measuring and Interpreting Point Spread Functions to Determine Confocal Microscope Resolution and Ensure Quality Control. *Nat. Protoc.* **2011**, *6,* 1929–1941.
38. Münster, S.; Fabry, B. A Simplified Implementation of the Bubble Analysis of Biopolymer Network Pores. *Biophys. J.* **2013**, *104,* 2774–2775.
39. Fritzsche, M.; Erlenkämper, C.; Moeendarbary, E.; Charras, G.; Kruse, K. Actin Kinetics Shapes Cortical Network Structure and Mechanics. *Sci. Adv.* **2016**, *2,* e1501337.
40. Morone, N.; Fujiwara, T.; Murase, K.; Kasai, R. S.; Ike, H.; Yuasa, S.; Usukura, J.; Kusumi, A. Three-Dimensional Reconstruction of the Membrane Skeleton at the Plasma Membrane Interface by Electron Tomography. *J. Cell Biol.* **2006**, *174,* 851–862.
41. Linsmeier, I.; Banerjee, S.; Oakes, P. W.; Jung, W.; Kim, T.; Murrell, M. P. Disordered Actomyosin Networks are Sufficient to Produce Cooperative and Telescopic Contractility. *Nat. Commun.* **2016**, *7,* 12615.
42. Gardel, M. L.; Valentine, M. T.; Crocker, J. C.; Bausch, A. R.; Weitz, D. A. Microrheology of Entangled F-Actin Solutions. *Phys. Rev. Lett.* **2003**, *91,* 158302.
43. Lieleg, O.; Claessens, M. M. A. E.; Bausch, A. R. Structure and Dynamics of Cross-Linked Actin Networks. *Soft matter* **2010**, *6,* 218–225.
44. Ershov, D.; Stuart, M. C.; van der Gucht, J. Mechanical Properties of Reconstituted Actin Networks at an Oil–Water Interface Determined by Microrheology. *Soft matter* **2012**, *8,* 5896–5903.
45. Head, D. A.; Levine, A. J.; MacKintosh, F. C. Distinct Regimes of Elastic Response and Deformation Modes of Cross-Linked Cytoskeletal and Semiflexible Polymer Networks. *Phys. Rev. E* **2003**, *68,* 61907.
46. Broedersz, C. P.; MacKintosh, F. C. Modeling Semiflexible Polymer Networks. *Rev. Mod. Phys.* **2014**, *86,* 995–1036.
47. Xu, J.; Palmer, A.; Wirtz, D. Rheology and Microrheology of Semiflexible Polymer Solutions: Actin Filament Networks. *Macromolecules* **1998**, *19,* 6486–6492.
48. Morse, D. C. Viscoelasticity of Concentrated Isotropic Solutions of Semiflexible Polymers. 2. Linear Response. *Macromolecules* **1998**, *31,* 7044–7067.
49. Hildebrandt, J. Comparison of Mathematical Models for Cat Lung and Viscoelastic Balloon Derived by Laplace Transform Methods from Pressurevolume Data. *B. Math. Biophys.* **1969**, *31,* 651–667.

TOC GRAPHIC: